Sensors and Materials, Vol. 36, No. 10 (2024) 4193–4204
MYU Tokyo

S & M 3794

Analysis and Design of NdFeB N35 Permanent Magnetic Holding Device Using ANSYS Maxwell Simulation

Lin Wang,[1] Che-Chia Tsao,[2] Chao-Ming Hsu,[2]
Cheng-Fu Yang,[3,4*] Ah-Der Lin,[5**] and Hsien-Wei Tseng[6]

[1]School of Electronic and Electrical Engineering, Zhaoqing University, Zhaoqing 526061, China
[2]Department of Mechanical Engineering, National Kaohsiung University of Science and Technology, Kaohsiung 807, Taiwan
[3]Department of Chemical and Materials Engineering, National University of Kaohsiung, Kaohsiung 811, Taiwan
[4]Department of Aeronautical Engineering, Chaoyang University of Technology, Taichung 413, Taiwan
[5]Department of Mechanical Engineering, Cheng Shiu University, Kaohsiung, 833, Taiwan
[6]College of Artificial Intelligence, Yango University, Fuzhou, Fujian 350015, China

(Received April 30, 2024; accepted August 30, 2024)

Keywords: stress and strain, intraocular pressure (IOP), fluid–structure interaction, applanation tonometry, ocular biomechanics

In this study, we investigated the integration of an NdFeB N35 permanent magnet into an electromagnetic chuck to maintain its magnetic force continuously. By energizing or de-energizing the coil wrapped around the chuck, the surface magnetic force was increased or decreased, achieving either stronger adhesion or easy detachment of the attached object, respectively. ANSYS Maxwell software was utilized to simulate the initial model, the results of which were then compared with physical measurements. Keeping the external dimensions unchanged, the yoke's dimensions were used as the parameters to analyze the effect of changes in dimensions at different positions on the electromagnetic chuck's surface adhesion force. Differences between simulated and measured results for the initial model after energizing the electromagnetic chuck were within 6%. Among the simulations with different parameters, changes in the thickness of the outer frame base and inner diameter did not significantly affect the magnetic flux on the surface of the electromagnetic chuck. Therefore, these results were not shown in this study. Alterations in the yoke's dimensions affected the relative position and size of the coil or created new magnetic flux paths. A distance of less than 1 mm between the coil and the chuck surface significantly affected the surface magnetic flux density.

1. Introduction

Electromagnets, which are capable of functioning as electromagnetic valves with low current flow, are utilized for magnetization and demagnetization by energizing and de-energizing, respectively, facilitating switch-like operations.[1,2] When a substantial current flows through the coil, generating a powerful magnetic field, the electromagnet not only serves as a control for

*Corresponding author: e-mail: cfyang@nuk.edu.tw
**Corresponding author: e-mail: 0549@gcloud.csu.edu.tw
https://doi.org/10.18494/SAM5105

ISSN 0914-4935

large valves but also doubles as a carrier for transporting bulky workpieces. Consequently, designing suitable electromagnetic suction cups becomes a critical issue. Optimizing the design ensures maximum attraction under fixed output power, leading to enhanced attraction effectiveness and higher power output efficiency. This, in turn, can significantly reduce production costs, making it a pivotal consideration in electromagnetic suction cup design. In modern society, companies are becoming increasingly meticulous in calculating costs. Particularly in this era, where every penny counts and precise calculations are necessary for everything, effectively reducing costs and improving efficiency have become crucial considerations. However, traditional electromagnetic lifters require power to function and generate waste heat during operation.

Permanent magnets are materials capable of maintaining their magnetism indefinitely and are typically composed of elements such as iron, cobalt, nickel, or their alloys. Because of their stable magnetic field, permanent magnets find applications in the manufacturing of various sensors including magnetic field sensors, speed sensors, position sensors, angle sensors, and flow sensors. These magnets serve as reliable sources of magnetic fields, enabling precise detection and measurement in a wide range of industrial, scientific, and automation applications. In the past, Sekino *et al.* developed a novel handheld magnetic probe with a magnetic sensor and a permanent magnet to detect sentinel lymph nodes in breast cancer patients.[3] One notable aspect of the probe was the precise positioning of its sensor at the magnetic null point of the magnet, resulting in highly sensitive measurements unaffected by the strong ambient magnetic fields. Niekiel *et al.* explored MEMS magnetic field sensors employing piezoelectric resonators driven by the interaction of integrated permanent magnets.[4] These sensors were crafted leveraging recent advancements in fabrication techniques to seamlessly integrate volumetric permanent magnets within MEMS structures.

To address this issue, in this study, we introduce NdFeB N35 permanent magnets into conventional electromagnetic lifters equipped with wound coils, enabling the lifter to retain magnetic force even when the coils are not energized.[5,6] By adjusting the degree of current flowing through the coils, the surface magnetic force can be increased or decreased to achieve stronger adhesion or easier detachment of objects, respectively. This design effectively reduces power consumption and heat generation. With the external form fixed and the magnetic properties unchanged, the performance of the lifter is further adjusted by modifying the shape of magnetic circuit components outside the magnets. Apart from the diameter and thickness of the magnet contact surface, we conduct simulation analyses on other dimensional parameters to understand their effects on surface magnetic flux density and adhesion force, thus identifying trends in their impact. Through these studies, the optimization of electromagnetic lifters can be better achieved, leading to improved performance and lower costs.

ANSYS Maxwell is a powerful electromagnetic field simulation software[7,8] boasting the following features.

(1) Electromagnetic field simulation capability: ANSYS Maxwell is capable of simulating static, steady-state, and variable-frequency electromagnetic fields, covering various electromagnetic phenomena such as electric fields, magnetic fields, electromagnetic induction, wire resistance, and electromagnets.

(2) Multiphysics coupling: In addition to electromagnetic fields, ANSYS Maxwell supports coupling simulations with other physical fields such as structural mechanics and thermal analysis. This enables models to comprehensively evaluate the impact of multiple physical effects.
(3) Multiscale simulation: It can handle various problems ranging from the microscale to macroscale, from small components to large systems.
(4) Visualization and post-processing: ANSYS Maxwell provides rich visualization tools and post-processing functionalities, allowing for intuitive analysis and presentation of simulation results.
(5) User-friendly interface: It offers an intuitive user interface and easy-to-use operation tools, enabling users to effortlessly model, set simulation parameters, and execute simulations.
(6) Accuracy and reliability: ANSYS Maxwell is one of the widely used electromagnetic field simulation tools in the industry and known for its high accuracy and reliability, making it capable of meeting the demands of various engineering applications.

During the process, ANSYS Maxwell is employed to simulate the initial model, and the parameters are compared with physical measurements for validation. In this study, we focused on the analysis and design of an NdFeB N35 permanent magnetic holding device using ANSYS Maxwell. Initially, relevant literature on electromagnetics, applications, and analysis was collected. Subsequently, fixed parameters and variables for the initial model were established. After the initial model was fabricated, Gauss meters were used to measure the gauss values at the surface center and inner and outer endpoints, providing a reference for simulated analysis. In the analysis with Maxwell, the collected data were inputted to analyze the initial model, and the simulation results were compared with the measured values to validate the accuracy of the data. Once the correctness of the data was confirmed, models for simulating various parameters were developed. The analysis results were then compiled, and a summary of the data was provided.

2. Methodology

In this study, we employed ANSYS Maxwell 16.0 for simulating and analyzing the experimental model. ANSYS Maxwell comprises three modules: RMxprt, Maxwell 2D, and Maxwell 3D, facilitating the analyses of 2D motor modules as well as the solving of electromagnetic field problems in both 2D and 3D domains. The software utilizes Maxwell's equations within finite spaces, with specified boundaries and initial conditions for resolution. The fundamental unit of finite elements was a tetrahedral mesh with 10 nodes, and each element employed second-order quadratic polynomials (basis functions) for approximation in calculations.

$$H_x(x,y,z) = a_0 + a_1x + a_2y + a_3z + a_4xy + a_5yz + a_6xz + a_7x^2 + a_8y^2 + a_9z^2 \quad (1)$$

In Maxwell 3D, basis functions were derived by extracting values from 10 nodes in the simulation (including vertices and edge nodes). Once tetrahedral elements were defined, finite

elements were placed within a large matrix. Present-day analysis software commonly employ the Gaussian elimination method for matrix solving. During the solving process, energy errors were calculated using Eq. (2). Maxwell iteratively refined the mesh by increasing grid density, which was based on the percentage error after each solving iteration, aiming for convergence.

$$\textit{Energy percentage error} = (\textit{error value}/\textit{total numerical value}) \times 100\% \quad (2)$$

Before commencing modeling and analysis in Maxwell 3D, the solver configuration was set, primarily distinguishing between magnetic and electric fields. For magnetic field analysis, options included static field, eddy current analysis, and transient analysis. Electric field options encompassed static field, direct-current conduction (including insulation), and transient field analyses. In the case of static magnetic field analysis, parameters such as relative permeability, volume conductivity, magnetic force magnitude, and magnetization direction need to be specified for materials. Consequently, boundary condition were established to delineate the field of solution, ensuring convergence by confining it within a defined domain instead of solving in infinite space. As depicted in Fig. 1, two types of boundary conditions were commonly utilized: Natural and Neumann. The Natural condition is applied to interfaces between objects, allowing magnetic fields to penetrate continuously through objects. Conversely, the Neumann condition ensures that the magnetic field tangentially interacts with the boundary box, confining magnetic flux within the designated area. In the meshing section of ANSYS Maxwell 16.0, all meshes were tetrahedral meshes. In simulating static magnetic fields, the solution involved setting up either a DC coil or a permanent magnet for analysis. The electric field effects of the current-carrying coil are excluded, with only resistive losses from the current contributing to losses. Moreover, the software automatically enhances computational precision by employing mesh refinement.

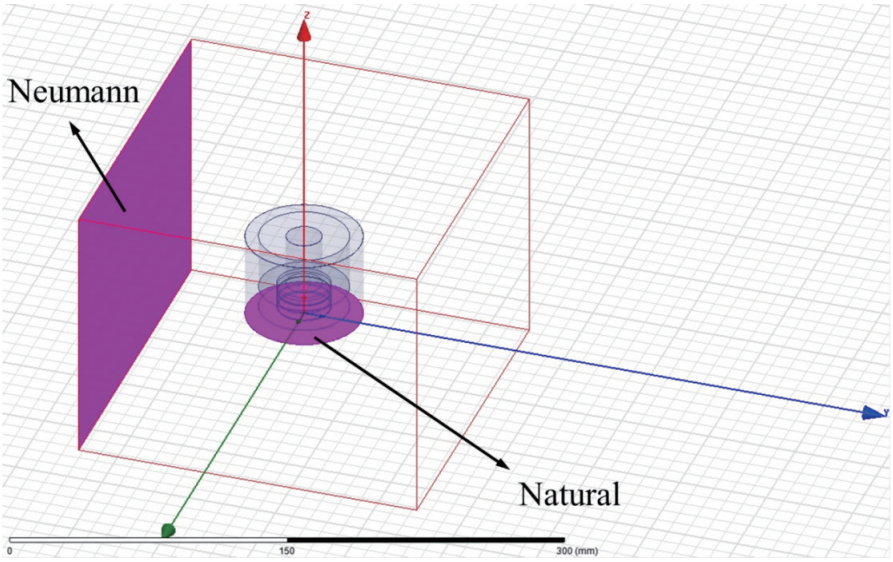

Fig. 1. (Color online) Boundary setting for Natural and Neumann setting positions.

The model used in this study is provided by Kinetic Motors Co., Ltd. Its structure involves permanent magnets embedded within an outer frame, around which coils are wound. This arrangement enables the suction cup to maintain magnetic adhesion even when power is disconnected. The model employs a cylindrical permanent magnet electromagnetic suction cup component, as shown in Fig. 2(a). The outer frame has a diameter (∅) of 65 mm and a height of 50 mm, with an inner circular groove of ∅55 mm and 45 mm depth. Internally, there is a magnetic yoke, two magnets, and a plastic ring. The purpose of the magnetic yoke is to conduct magnetic force from the magnets to the exterior of the suction cup, while the plastic ring ensures alignment of the magnets and the yoke at the center of the outer frame. The fully assembled model is depicted in Fig. 2(b). The outer frame and magnetic yoke in this experiment are made of AISI 1020 low-carbon steel, while the permanent magnets are made of neodymium iron boron material, specifically, NdFeB N35-grade circular permanent magnets.

In this study, we enhanced the magnetic effect of the entity by embedding permanent magnets and winding coils to increase or decrease the magnetic force. A power supply converted household 110 V AC to DC, and a clamp meter was used to measure the current passing through the coils. For measurement, a Gauss meter was employed to measure the magnetic flux density on the adhesive surface. After constructing the physical model, the measured magnetic flux density on the electromagnetic disk surface was used to determine the parameters for simulation analysis. A comparison between measured data and analytical values was conducted. Also, in this study, we measured the surface magnetic flux of magnets, electromagnetic disks with winding, and electromagnetic disks without winding. Three experiments were conducted, measuring values at eight points equally distributed at 45° intervals along the circumference at different measurement positions, with standard deviation calculated from the averages. Magnet measurement involved adhering two N35 magnets together and measuring the magnetic field strength at the center and edges using a Gauss meter.

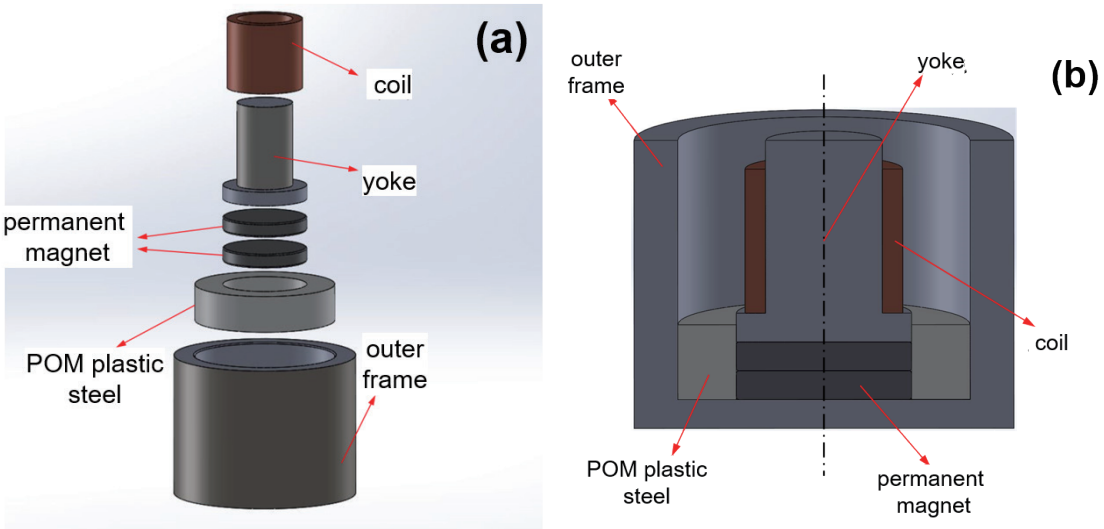

Fig. 2. (Color online) Permanent magnet electromagnetic chuck model: (a) exploded graph and (b) cutaway view of assembled model.

The simulation parameters were as follows: the bottom thickness of the outer frame was 5 mm; the inner diameter of the outer frame was 50 mm; the yoke bottom thickness varied in the range of 3–7.5 mm; the yoke bottom diameter varied in the range of 20–50 mm in steps of 5 mm; the yoke shaft diameter varied in the range of 5–40 mm; the yoke top width varied in the range of 20–50 mm; the yoke bottom chamfer varied in the range of 0–45°; the number of coil turns was 2000; and the voltage was 24 V. Regarding the average magnetic flux density on the magnet surface, the central value was 2258 gauss, and the edge value was 5226 gauss. For the surface measurements of the unwound disk, as shown in Fig. 3, the gauss values at points A, B, C, and D were 1054, 3718, 767, and 190 gauss, respectively. For the surface measurements of the disk wound with 2000 turns of the coil, as shown in Fig. 3, the gauss values at points A, B, C, and D were 1361, 4529, 1159, and 219 gauss, respectively.

After completing the initial model construction and measurements, the model was created as a 3D assembly in SolidWorks and saved as an .x_t file. ANSYS Maxwell was then opened, and a Maxwell 3D program was selected to import the file for simulation analysis. The convergence plot of the mesh for the magnetic disk indicated stability with around 1897292 elements. At this point, the maximum node spacing for the magnetic yoke, magnet, and coil models was set to 1.4 mm, while for the outer frame, it was set to 1.3 mm. The plastic steel node spacing was set to a maximum of 10 mm. With these settings, the outer frame had the most meshes, a total of 1247152, followed by the magnetic yoke with 168296 meshes. Subsequently, analytical precision and post-processing interfaces were configured. In the analysis settings, convergence error percentage, mesh adaptation refinement rate, and maximum analysis step length were specified. For this study, we set the calculation error to 1%, mesh adaptation refinement rate to 5%, and maximum step length to 30 steps to ensure analysis convergence during software verification. In post-processing, a cross-sectional view of the magnetic flux density distribution was observed

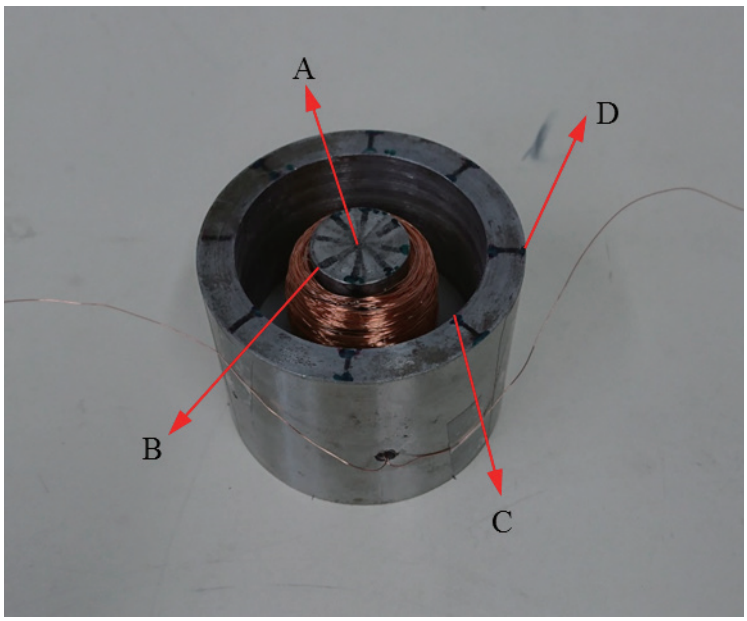

Fig. 3. (Color online) Measurement positions without and with coil.

across the entire section. The internal field calculator was then utilized to retrieve the analysis results for the magnetic flux density on the surface of the electromagnetic disk.

3. Simulation Results and Discussion

The simulation results revealed the magnetic flux densities of the electromagnetic disk without copper winding and with 2000 turns of winding carrying a current of 0.27 A. Through simulations using solely a magnet, the software's magnet material parameters were validated. The simulated magnetic flux density at the magnet's center was 2157 gauss, with a 4.7% error compared with the measured value of 2258 gauss. At the magnet's edge, the simulated average was 5456 gauss, with a 1.3% error compared with the measured average of 5526 gauss. In the electromagnetic disk without winding, both measurement and simulation results indicated the highest magnetic flux density at the edge of the yoke (point B). This model was used to verify the hysteresis curve parameters of the AISI 1020 low-carbon steel used for the frame and yoke. The simulated magnetic flux density results at points A, B, C, and D averaged 1106, 3481, 761, and 180 gauss, respectively, with errors of 4.9, 1.0, 0.7, and 5.6% compared with the measured values. For the electromagnetic disk with 2000 turns of the coil carrying a current of 0.27 A, the simulated magnetic flux densities at points A, B, C, and D averaged 1286, 4801, 1146, and 216 gauss, respectively, with errors of 5.8, 6.0, 1.1, and 1.7% compared with the measured results. The coil in the model was constructed on the basis of the actual dimensions of a measured 2000-turn coil, using a simplified approximation. The current through the coil was adjusted on the basis of the resistance of the copper wire, compared with the ideal current value, to account for discrepancies between actual measurements and theoretical values. Through comparisons of the overall error using this model, it was observed that the error in the yoke was slightly larger than that in the frame.

In this study, we primarily investigate the effects of various parameters of the yoke on the simulation results. Table 1 lists the simulated results for different yoke bottom thicknesses. Up to a thickness of 9 mm, there is no significant change in the magnetic flux density on the disk surface. The magnetic flux density at each point shows only a slight decrease, with the maximum variation observed at point B, fluctuating between 4578 and 4834 gauss. After 9 mm, there is a significant increase in the magnetic flux density at point B, while the other three points continue

Table 1
Simulated results of surface magnetic flux density (unit: gauss) for different yoke bottom thicknesses.

Yoke thickness (mm)	A	B	C	D
3	1300	4742	1132	223
4	1277	4834	1117	222
5	1286	4801	1146	216
6	1275	4691	1090	218
7	1298	4616	1078	214
8	1296	4578	1099	206
9	1267	4639	1056	200
9.5	1261	5011	1073	206
10	1258	5572	1042	207

to exhibit a decreasing trend. In a one-factor experiment, all parameters other than the variable parameter remained constant. Under this parameter variation, as the thickness of the yoke increases, the coil model moves closer to the magnet surface. Figure 4 illustrates the simulated results for different yoke bottom thicknesses. As the yoke becomes thicker, the induced magnetic field from the yoke gradually rises to the surface of the disk. When the yoke bottom thickness reaches 9 mm, the top of the coil model is 1 mm away from the disk surface. At a yoke bottom thickness of 10 mm, the top of the coil model is flush with the surface, that is, at a distance of 0 mm. This parameter variation also reveals another result: when the coil is less than 1 mm away from the surface of the electromagnetic disk, the magnetic field generated by the coil's current can directly affect the surface performance.

Table 2 shows the simulated results for different diameters of the yoke bottom. From the numerical data, it can be observed that the optimal surface magnetic flux density at points A to D is achieved when the bottom diameter is 25 mm, with values of 1328, 4858, 1158, and 217.88 gauss, respectively. Between bottom diameters of 20 and 30 mm, there is no significant variation in the magnetic flux density at points A, B, and C. However, beyond 30 mm, there is a decreasing trend in the magnetic flux density at these three points, with point B showing a particularly noticeable decline. Figure 5 illustrates the simulated results for different yoke bottom diameters. As the yoke bottom diameter increases, the magnetic flux density approaches closer to the inner edge of the frame. When the magnet diameter is 30 mm, if the yoke bottom diameter exceeds the magnet diameter, the surface magnetic flux density begins to decrease. When the bottom diameter reaches 50 mm, a magnetic loop is formed internally, preventing the magnetic field from reaching the surface of the disk directly. This indicates that excessively large bottom diameters do not enhance the surface performance of the electromagnetic disk.

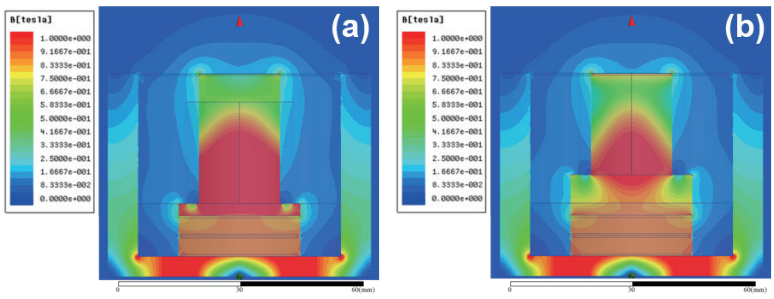

Fig. 4. (Color online) Simulated results for different yoke bottom thicknesses: (a) 3 and (b) 10 mm.

Table 2
Simulated results of surface magnetic flux density (unit: gauss) for different yoke bottom diameters.

Yoke bottom diameter (mm)	A	B	C	D
20	1228	4613	1049	205
25	1328	4858	1158	218
30	1286	4801	1146	216
35	1163	4149	989	200
40	1025	3705	860	171
45	791	2914	704	130
50	407	1470	331	62.9

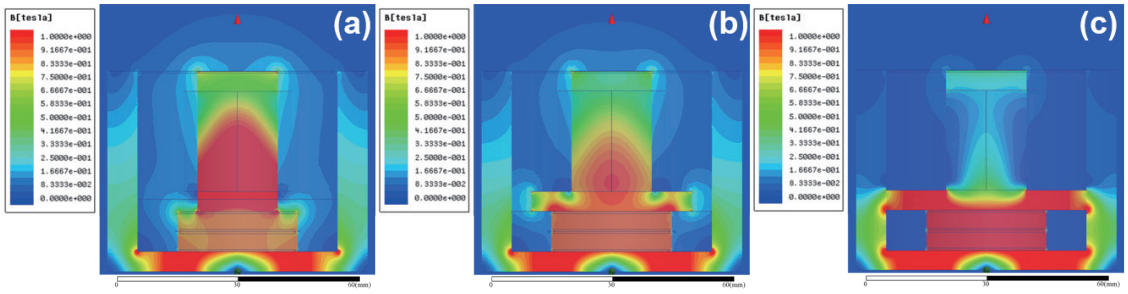

Fig. 5. (Color online) Simulated results for different yoke bottom diameters: (a) 20, (b) 40, and (c) 50 mm.

Table 3 shows the simulated results for different yoke shaft diameters. From the table, it can be seen that the yoke exhibits higher magnetic flux density at diameters of 10 and 15 mm, followed by a gradual decrease. The magnetic flux density at points C and D of the frame, however, steadily increases with the increase in yoke shaft diameter. Typically, the magnetic flux density at point C, located at the inner periphery of the frame, is slightly lower than that at the center point A of the yoke. However, starting from a shaft diameter of 25 mm, the magnetic flux density at point C begins to exceed that at the yoke center, with the difference becoming substantial as the diameter increases. As the yoke shaft diameter increases, the required winding radius for the coil also increases, bringing the coil closer to the frame. The magnetic field generated by the coil increases the magnetic flux density of the frame gradually. In Fig. 6, it can be observed that an appropriately sized diameter allows the magnetic field to have a wider range of influence. Diameter sizes that are too large or too small only affect areas close to the surface, but a larger diameter yoke can provide a more uniform magnetic flux density on the surface of the disk.

Table 4 shows the simulation results of surface magnetic flux for different sizes of the yoke cap. Similar to changing the yoke shaft diameter, altering the yoke cap size results in different load-bearing areas on the surface of the disk. The difference lies in the fact that changing the entire shaft diameter compresses the winding space of the coil and increases the weight of the electromagnetic disk itself. From the results in Table 4, it can be seen that, except at point C, larger caps result in lower magnetic flux density at other positions. Figure 7, which shows the simulated results for different cap parameters, illustrates that larger caps bring points B and C closer together, reducing the air gap between them. Consequently, the magnetic flux density at point C gradually increases. When the cap diameter reaches 50 mm, the yoke effectively contacts the frame, forming a complete magnetic loop that causes direct conduction within the low-carbon steel with minimal flux leakage into the atmosphere. This outcome is clearly visible from the color distribution in Fig. 7. From the results of this subparameter analysis, it can be inferred that when transporting magnets, aside from maintaining a distance from other magnetically conductive materials, using containers made of materials with higher magnetic permeability can also shield the magnetic field from leaking externally.

Table 5 lists the simulation results for different angles of the yoke bottom chamfer, when the parameter settings were based on commonly used chamfer angles in engineering practice.

Table 3
Simulated results of surface magnetic flux density (unit: gauss) for different yoke shaft diameters.

Yoke shaft diameter (mm)	A	B	C	D
5	1755	3210	270	47.3
10	1893	5044	550	109
15	1696	5457	885	172
20	1286	4801	1146	216
25	1016	4293	1318	237
30	794	4539	1616	292
35	598	3718	1768	282
40	451	3587	2170	262

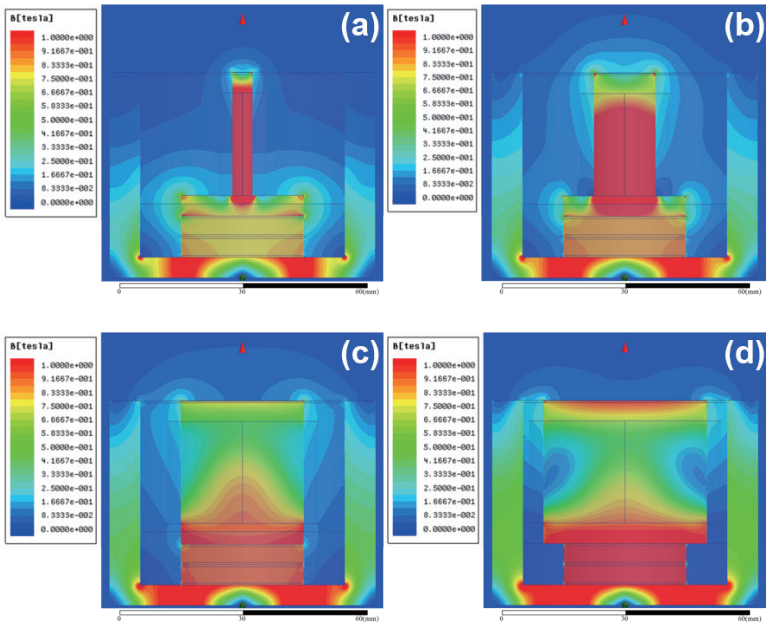

Fig. 6. (Color online) Simulated results for different yoke shaft diameters.

Table 4
Simulated results of surface magnetic flux density (unit: gauss) for different yoke cap sizes.

Yoke cap size (mm)	A	B	C	D
20	1286	4801	1146	26
30	828	4209	1579	283
40	504	3717	2318	291
45	346	3686	2784	243
50	116	114	11.4	3.50

Figure 8 depicts the simulated results for different chamfer angles. In the simulated results of different parameters, it was observed that there is lower magnetic flux density at the junction between the yoke bottom and the yoke shaft, and higher values on the outer side, resembling an eddy current phenomenon. Increasing the chamfer angle is explored as a means to potentially improve this condition and enhance the surface magnetic performance. However, from the curve

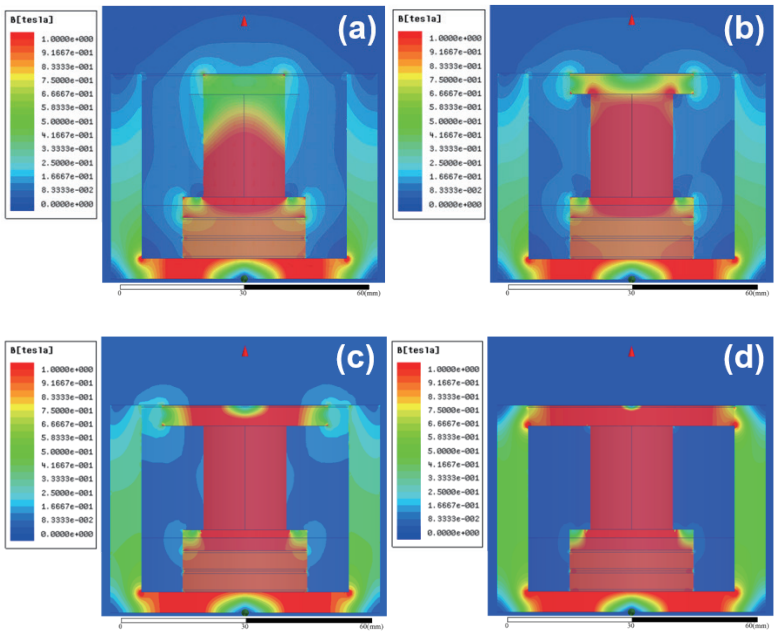

Fig. 7. (Color online) Simulated results for different sizes of yoke cap: (a) 20, (b) 30, (c) 40, and (d) 50 mm.

Table 5
Simulated results of surface magnetic flux density (unit: gauss) for different yoke bottom chamfer angles.

Yoke chamfer angle (°)	A	B	C	D
0	1286	4801	1146	216
15	1330	4822	1110	223
30	1350	4875	1136	224
45	1344	4965	1192	223

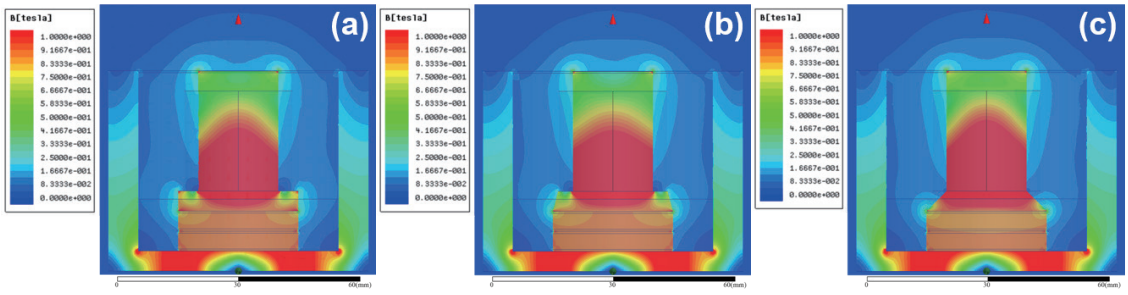

Fig. 8. (Color online) Simulation results for yoke bottom chamfer at different angles: (a) 0°, (b) 15°, and (c) 45°.

variations and simulated results, we inferred that although the eddy current phenomenon may be alleviated by increasing chamfer angles, there is almost no effect on the magnetic flux on the surface, and there is little change in the induced magnetic field range.

4. Conclusions

In this study, we focused on the optimization of a cylindrical permanent magnet electromagnetic chuck while keeping the maximum dimensions and magnet specifications constant, with alterations made to the dimensions of the magnetic yoke. Under fixed power conditions, simulations were conducted using a one-factor-at-a-time experimental approach to analyze how changes in the structure of the magnetic yoke affect the magnetic flux density at the surface of the electromagnetic chuck, thus gaining an understanding of the impact of these parameters. When the bottom thickness of the magnetic yoke exceeds 9 mm, the coil distance from the surface is less than 1 mm, which begins to affect the surface, resulting in an increase in the magnetic flux density at the edge of the yoke. However, increasing the bottom diameter and the shaft diameter of the magnetic yoke does not significantly increase the magnetic flux density at the surface of the electromagnetic chuck. This is primarily because a magnetic loop forms inside the chuck, whereby the magnetic flux does not pass through the adsorption surface. Moreover, as the shaft diameter of the magnetic yoke increases, the coil moves closer to the inner diameter circle of the frame, causing the magnetic flux originally derived from the yoke to disperse outward through the frame. Additionally, simply adding a top cover to increase the surface area of the chuck may enhance the magnetic flux density at the inner diameter position of the frame; however, the overall effect is diminished, and the range influenced by the magnetic field is reduced. At the junction between the bottom and shaft of the magnetic yoke, there is a phenomenon similar to eddy currents, resulting in a lower distribution of magnetic flux density. The edges of the bottom of the yoke exhibit higher magnetic flux density, indicating that some of the magnetic flux flows from there to the frame. Adjusting the curvature at the bottom can improve the loop of magnetic flow, thereby enhancing the surface performance of the chuck, but the effect is not significant.

Acknowledgments

This research was funded by Zhaoqing Science and Technology Innovation Guidance Project, grant number 2022040304005 and supported by Summit-Tech Resource Corp. and by the Great project of production, teaching, research of Fujian provincial Science and Technology Department (2023H6025).

References

1 https://testbook.com/physics/uses-of-electromagnet (accessed January, 2024).
2 https://www.vedantu.com/physics/principal-applications-of-electromagnet (accessed February, 2024).
3 M. Sekino, A. Kuwahata, T. Ookubo, M. Shiozawa, K. Ohashi, M. Kaneko, I. Saito, Y. Inoue, H. Ohsaki, H. Takei, and M. Kusakabe: Sci. Rep. **8** (2018) 1195.
4 F. Niekiel, J. Su, M. T. Bodduluri, T. Lisec, L. Blohm, I. Pieper, B. Wagner, and F. Lofink: Sens. Actuators, A **297** (2019) 111560.
5 X. Luo, Q. Qiu, L. Jing, D. Zhang, P. Huang, and S. Jia: 2022 IEEE 5th Int. Electrical and Energy Conf. (CIEEC, 2022) 3121–3126.
6 https://www.albmagnets.com/blog/ndfeb-n35-n35sh-magnets.html (accessed March, 2021).
7 N. C. Tsai, J. S. Liou, C. C. Lin, and T. Li: Sens. Actuators, A **157** (2010) 68.
8 N. C. Tsai and C. W. Chiang: Mechatronics **20** (2010) 596.